Polarization spectra of Zeeman sublevels in Rydberg electromagnetically induced transparency

Shanxia Bao, Hao Zhang, Jian Zhou, Linjie Zhang, Jianming Zhao, Liantuan Xiao, and Suotang Jia

Phys. Rev. A **94**, 043822 — Published 14 October 2016

DOI: 10.1103/PhysRevA.94.043822

Polarization Spectra of Zeeman Sublevels in Rydberg Electromagnetically Induced Transparency

Shanxia Bao[1,2], Hao Zhang[1,2], Jian Zhou[1,2], Linjie Zhang[1,2,*] Jianming Zhao[1,2], Liantuan Xiao[1,2], and Suotang Jia[1,2]
[1] *State Key Laboratory of Quantum Optics and Quantum Optics Devices, Institute of Laser Spectroscopy, Shanxi University, Taiyuan 030006, China and*
[2] *Collaborative Innovation Center of Extreme Optics, Shanxi University, Taiyuan 030006, China*

The polarization spectra of electromagnetically induced transparency (EIT) for Zeeman sublevels in a cascade system with Rydberg state are demonstrated. The magnitude dependence of Rydberg-EIT on the polarizations of probe and coupling laser fields is studied, and shown mainly due to the strengths of relative dipole matrix elements between degenerate Zeeman sublevels. We further investigate the polarization spectra of Rydberg-EIT in the optimal polarization combinations of left-handed and right-handed circularly polarized fields when an external magnetic field is applied. The existence of nondegenerate Zeeman sublevels in external magnetic field results in the splitting of Rydberg-EIT. The theoretical calculations are consistent well with the experimental spectra.

PACS numbers: 32.80.Ee, 42.50.Gy, 32.60.+i, 42.25.Ja
Keywords: Rydberg EIT,polarization spectra,Zeeman sublevels

I. INTRODUCTION

Electromagnetically induced transparency (EIT) is a phenomenon that a weak probe field will experience increased transmission in an absorbing medium under a strong coupling field. As a typical quantum interference effect [1], it has been extensively investigated theoretically and experimentally. Since the EIT was first proposed [2] and demonstrated [3], it has been observed in atomic vapor [4], cold atom [5], Bose Einstein condensate [6] and has attracted widespread attention with a variety of interesting and important applications, such as enhancement of nonlinear optical effects [7, 8], slow light [9], photon storage [10, 11], and precision magnetometer [12, 13].

The research about EIT also was extended to the cascade-type system, for example, Rydberg atoms. These highly excited atoms with principal quantum number $n \gg 1$ [14] are attractive in field meteorology due to their strong response to applied external fields(polarizabilities typically scale$\sim n^7$) [15–17], also in quantum information or nonlinear optics in view of their very long coherence times and strong dipole-dipole interaction [18–21].J.Clarke *et al.* have observed EIT in a mismatched system with highly excited states (only for low quantum numbers) and demonstrated an optical switch [22]. C.S.Adams *et al.* firstly demonstrated a direct nondestructive probe of highly excited Rydberg states using EIT in vapor cells [23]. Weatherill *et al.* have observed a giant electro-optic effect using polarizable dark states in a Rydberg-EIT medium, which enable precision electrometry [24]. M. Müller *et al.* have presented a theoretical demonstration of a parallelized CNOT gate based on EIT in a strongly interacting Rydberg atoms system [25].H. Gorniaczyk *et al.* have realized single-photon transistor by mapping gate and source photons into strongly interacting Rydberg excitation in an ultracold atomic ensemble [26].Recently,it has been shown that polarization could play important roles in Rydberg-EIT. For instance,the polarization spectra of Rydberg-EIT in a vapor cell were used for vector microwave electrometry [17] and polarization of optical fields could affect the intrinsic bistability in a thermal Rydberg gas [27]. Especially combining with the Zeeman Effect, considering the exaggerated characteristics of Rydberg atoms above mentioned, which will be meaningful in precision magnetometer.

In this paper, we investigate the polarization spectra of Rydberg-EIT between Zeeman sublevels of a cascade system formed with ground state $6S_{1/2}$, intermediate state $6P_{3/2}$ and Rydberg state $nS_{1/2}$ in a temperature-controlled ^{133}Cs vapor cell. The magnitude dependence of Rydberg-EIT on the probe and coupling field polarizations are demonstrated. It is shown that the different strengths of relative dipole matrix elements between degenerate Zeeman sublevels are mainly responsible for the dependence. Further, the polarization spectra of Rydberg-EIT with an external magnetic field are observed. The existence of nondegenerate Zeeman sublevels when an external magnetic field is applied will induce the splitting of Rydberg-EIT. What's more, the polarization spectra is compared with theoretical calculation considering the relative dipole matrix elements, electric dipole approximation and rotating wave approximation.

II. THEORETICAL ANALYSIS

Here, we consider an ideal cascade three-level system formed by a rapidly decaying state, intermediate state $|2\rangle$, $6P_{3/2}$(F'=5), and two long lived states, ground state $|1\rangle$, $6S_{1/2}$(F=4) and Rydberg state $|3\rangle$, $nS_{1/2}$(F=4) as shown in Fig.1(a), the Hamiltonian of the system can be

*Corresponding author: zlj@sxu.edu.cn

written as

$$H = H_0 + H_1 \tag{1}$$

where H_0 is the unperturbed Hamiltonian, H_1 is the interaction between light and atoms.

Considering the rotating-wave approximation, and then expanding the Hamiltonian in the space of $|1\rangle$, $|2\rangle$, $|3\rangle$ as

$$H = \begin{pmatrix} 0 & \Omega_p & 0 \\ \Omega_p & -2\Delta_p & \Omega_c \\ 0 & \Omega_c & -2(\Delta_p + \Delta_c) \end{pmatrix} \tag{2}$$

in which Ω_p and Ω_c are the Rabi frequencies of probe and coupling fields, and Δ_p=ω_{12}-ω_{0p}, Δ_c=ω_{23}-ω_{0c} are the detunings of the probe and coupling fields, respectively, where ω_{12} and ω_{23} are the transition frequency of probe field and coupling field, ω_{0p} and ω_{0c} correspond to the resonant frequency of $6S_{1/2}$(F=4, m_F=0)$\rightarrow$$6P_{3/2}$(F=5, m_F=0) and $6P_{3/2}$(F=5, m_F=0)$\rightarrow$$nS_{1/2}$(F=4), respectively.The Rabi frequency of probe and coupling fields can be generally expressed as

$$\Omega = \frac{\mu_{ij}}{\hbar}\sqrt{\frac{2P}{\pi\omega^2 c\varepsilon_0}} \tag{3}$$

Here μ_{ij} is the dipole matrix element between two states $|i\rangle$ and $|j\rangle$, P is the power of the laser coupling the transition and ω is the waist radius of laser beam. From a density matrix analysis, the system can be described using the motion equation of the density matrix ρ:

$$\dot{\rho} = -\frac{i}{\hbar}[H, \rho] + \Gamma \tag{4}$$

where Γ refers to the dissipation and dephasing of the three level system [28].

The steady-state solution for the density matrix equations, with the electric dipole approximation and the rotating wave approximation, in the weak probe limit, is expressed as

$$\rho_{21} = -\frac{i\Omega_p/2}{\gamma_{21} - i\Delta_p + \frac{\Omega_c^2/4}{\gamma_{31} - i(\Delta_p + \Delta_c)}} \tag{5}$$

Here γ_{ij} =(Γ_i+Γ_j)/2 +γ_i/2 is the decay rates, where Γ_i is the natural decay rate of level $|i\rangle$ (with Γ_1=0) and γ_i is decay rate related to the interaction between ground-state atoms (i=2) or Rydberg atoms (i=3). γ_2 can be neglected compared to Γ_2, while γ_3 is the dominant contribution to the dephasing of the Rydberg state.

Considering the Doppler broadening effect, an atom moving towards the probe beam with velocity v "sees" its frequency upshifted by an amount $\omega_p v/c$, while the frequency of the coupling beam is, for the same atom, downshifted by an amount $\omega_c v/c$. Due to the quite different wavelengths of the probe and coupling beams, we also need consider the Doppler shifts that are only partially compensated by the counter-propagating beams. The complex susceptibility χ, its imaginary part indicate the absorption characteristic of the atomic medium, is modified as [29]

$$\chi(v)dv = \frac{i\mu_{21}^2/\varepsilon_0\hbar}{\gamma_{21} - i\Delta_p - i\frac{\omega_p}{c}v + \frac{\Omega_c^2/4}{\gamma_{31} - i(\Delta_p + \Delta_c) - i(\omega_p - \omega_c)v/c}} N(v)dv \tag{6}$$

with $N(v)dv$=$N_0\exp(-v^2/u^2)/(u\sqrt{\pi})dv$ is the number of atoms per unit volume with velocity v, where u is the most probable speed of atoms at given temperature. Then we can integrate $\chi(v)$ for getting the probe transmission.

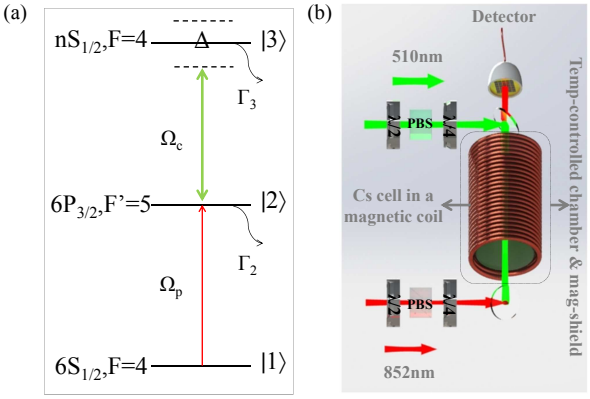

FIG. 1: (Color online) (a) Sketch of the Rydberg-EIT cascade system. A probe beam (Rabi frequency Ω_p) is applied to the $6S_{1/2}$(F=4) $\rightarrow$$6P_{3/2}$(F'=5) transition and coupling beam (Rabi frequency Ω_c and detuning $\triangle$) is the $6P_{3/2}$(F'=5)$\rightarrow$$nS_{1/2}$(F=4) transition. Γ_2 and Γ_3 are the nature decay rates of the $6P_{3/2}$ and Rydberg state, respectively. (b) Sketch of the experimental setup. The 852nm probe beam and 510nm coupling beam are counter-propagated and focused in the center of cell, which is in a magnetic coil, temperature-controlled chamber and multi-layer shield. The combinations of $\lambda/2$ (half-wave plate), PBS (polarizing beam splitter) and $\lambda/4$ (quarter-wave plate) in probe and coupling light paths before entering the cell can guarantee any polarization combinations.

III. EXPERIMENTAL SETUP

The Rydberg-EIT experiments are performed in a ^{133}Cs vapor cell at a controlled temperature of 300K. The $6P_{3/2}$ and $nS_{1/2}$ are strongly coupled and transmissions are detected via probe laser resonance in $6S_{1/2}\rightarrow6P_{3/2}$ transition. The probe beam, provided by an extended-cavity diode laser (DL100, Toptica) with the wavelength of 852nm, is locked on an High-Finesse Fabry-Perot cavity with ultra-low thermal expansion (ULE) glass (ATF-6010-4, Stable laser system), which has a guaranteed finesse $\approx2\times10^5$ and a high stability due to the vacuum

housing ($<10^{-6}$Pa) and temperature control (52.63°C). The linewidth of probe laser is smaller than 100KHz.The free spectral range of this cavity is 1.5GHz. The probe laser is locked on the ULE cavity at the frequency closed to the $6S_{1/2}(F=4)\rightarrow 6P_{3/2}(F'=5)$ resonance transition, and then is shifted to the resonance transition by a double-passed acoustic-optical modulator (AOM). The 0 order and 1^{st} order diffraction lights are simultaneously introduced into the vapor cell. We can observe two EIT signals with a fixed separation corresponding to the frequency shift of AOM, which is used as an accurate frequency standard to calibrate the EIT spectra. The coupling beam with the wavelength of 510nm, driving the transition of $6P_{3/2}(F'=5)\rightarrow nS_{1/2}(F=4)$, is provided by a doubled-frequency laser system (TA-SHG pro, Toptica). The probe beam has a waist 80μm and power 1.0μW, 100μm and 10mW for coupling beam. The probe beam is detected with a fast photodetector (PDA36A-EC, Thorlabs). The method that locked the probe beam and monitored its transmission while scanning the coupling beam makes transmission appear on a flat background and doesn't have an underlying Doppler profile that may cause undesirable peak-pulling effect [30].

The sketch of experimental setup is shown in Fig.1 (b). The ^{133}Cs atomic vapor cell, 4cm long and 2cm in diameter, is contained in a cylindrical copper coil with 211×3 turns. The uniform magnetic field in the axis of vapor cell is produced by the cylindrical copper coil, with length 25cm and diameter 5cm.The magnetic field can be scanned linearly, from 0 to 100G, with the uncertainty of less than 0.1G. They are placed in a temperature-controlled chamber of 300K and magnetic shield materials around avoiding the influence of stray magnetic field. The probe and coupling beams are collinearly counter-propagated and focused in the center of cell. Both the two beams pass through a half-wave plate ($\lambda/2$), a polarizing beam splitter (PBS) and a quarter-wave plate ($\lambda/4$) before entering the cell, and then we can obtain any different polarization combinations of probe and coupling laser fields.

IV. EXPERIMENTAL RESULTS AND DISCUSSION

A. Polarization spectral of Rydberg-EIT

We observe firstly the Rydberg-EIT spectra for nine polarization combinations of probe and coupling fields, with π representing linearly polarized light; σ^+, left-handed circularly polarized light; σ^-, right-handed circularly polarized light. As shown in Fig.2(a), (b), the Rydberg state is $49S_{1/2}$ and $46S_{1/2}$, respectively. The polarization combinations labeled in Fig.2 represent the polarization of probe field–the polarization of coupling field. It should be noted that if both the probe and coupling laser fields are set as the same circular polarization, then the atomic sample will "experience" the opposite circular polarization since the two beams are counter-propagated, and the polarization "experienced" by the atomic sample are used in our analysis. It is clearly shown that the Rydberg-EIT spectra depend on the relative polarization combination of the applied optical fields.

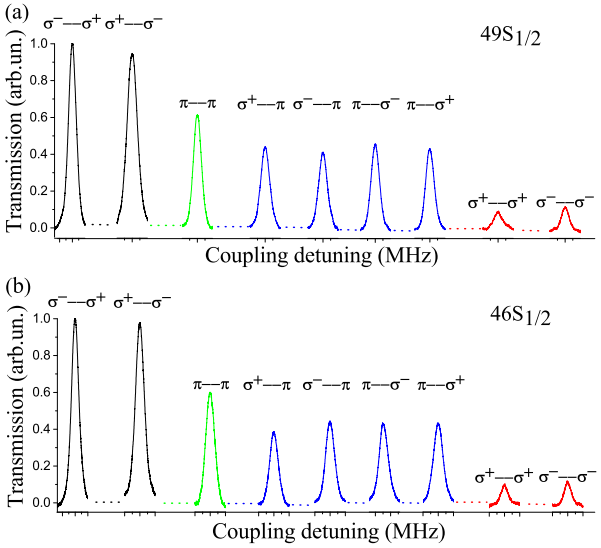

FIG. 2: (Color online) Rydberg-EIT spectra when different polarization combinations of probe and coupling fields are used. The polarization combinations represent probe field polarization–coupling field polarization. The level $|3\rangle$ is $49S_{1/2}$ Rydberg state for (a) and $46S_{1/2}$ Rydberg state for (b).

The degenerate Zeeman sublevels and strength of relative dipole matrix elements between the Zeeman sublevels are responsible for the difference of polarization spectra [31]. The strength of the interaction between two Zeeman sublevels is characterized by the dipole matrix elements [32]:

$$\begin{aligned}\langle IJFm_F \ \ |er_q| \ \ I'J'F'm'_F\rangle &= (-1)^{F'-1+m_F}\sqrt{2F+1}\begin{pmatrix} F' & 1 & F \\ m'_F & q & -m_F\end{pmatrix} \\ &\times (-1)^{F'+J+1+I}\sqrt{(2F'+1)(2J+1)} \\ &\times \begin{Bmatrix} J & J' & 1 \\ F' & F & I\end{Bmatrix}\langle J\|er\|J'\rangle \end{aligned} \quad (7)$$

Here, I is the nuclear spin (I=7/2 for ^{133}Cs), J is the angular momentum, F is the total angular momentum and m_F is the Zeeman sublevels. The primed variables refer to the final states and unprimed variables correspond to the initial states in which the atom resides. The value of q is polarization dependent, with $q=m_F-m'_F$.The $\langle J\|er\|J'\rangle$ is reduced matrix element and can be factored out if one considering only the relative dipole matrix strengths, as our case. The values in the parentheses and curly brackets denote the Wingner 3-j symbol and Wingner 6-j symbol, respectively.

Then we can calculate the relative transition strengths between two m_F levels just using (without evaluating the

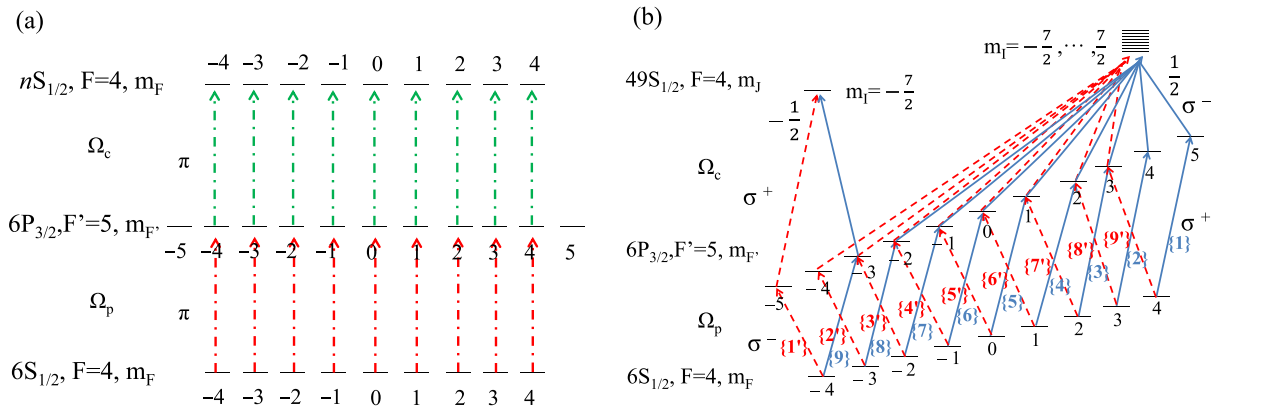

FIG. 3: (Color online) (a) Degenerate Zeeman sublevels of cascade system coupled by linear polarized laser fields. (b) All possible transitions between nondegenerate Zeeman sublevels coupled by circular polarized fields in the presence of an axial static magnetic field.Each number of {1}–{9} represents a corresponding transition,respectively. σ^-–σ^+ polarization combinations (red dashed line and primed numbers), and σ^+–σ^- polarization combinations (blue solid line and unprimed numbers).

TABLE I: Measured and calculated (Cal.) relative transition strengths in all the nine polarization combinations for Rydberg state being $49S_{1/2}$ and $46S_{1/2}$, respectively, normalized against the largest value.

Probe polarization	Coupling polarization	$49S_{1/2}$	$46S_{1/2}$	Cal.
σ^-	σ^+	1.00	1.00	1.00
σ^+	σ^-	0.94	0.97	1.00
π	π	0.62	0.59	0.68
σ^+	π	0.44	0.38	0.42
σ^-	π	0.42	0.44	0.42
π	σ^-	0.46	0.43	0.42
π	σ^+	0.43	0.43	0.42
σ^+	σ^+	0.09	0.10	0.09
σ^-	σ^-	0.11	0.12	0.09

reduced matrix element $\langle J\|er\|J'\rangle$)

$$S = |\langle IJFm_F|er_q|I'J'F'm'_F\rangle|^2 \tag{8}$$

We are able to calculate the transition strengths in a given polarization combination by appropriate addition and multiplication, due to each transition is independent of the others, such as Fig.3 (a) ,the case of linear-linear polarization combination. As shown in Table.I, the measured relative transition strengths for Rydberg state $49S_{1/2}$ and $46S_{1/2}$ in all the nine polarization combinations are compared with calculated values, normalized against the largest value. The errors, maximum 9%, between measured and calculated data attribute to the imperfect polarization prepared in experiments and optical pumping effect.

B. Polarization spectral of Rydberg-EIT in external magnetic field

We investigate further the polarization spectra of nondegenerate Zeeman sublevels in the cascade-type system, the uplevel is $49S_{1/2}$ Rydberg state, in the optimal polarization combinations of σ^+–σ^- and σ^-–σ^+ based on section A. For an ideal three-level system, the degeneracy of all three energy levels will be broken while a static magnetic field is applied. The splittings of Rydberg-EIT spectra are observed because of the existence of nondegenerate Zeeman sublevels. The measured polarization spectra in σ^+–σ^- and σ^-–σ^+ cases with different magnetic fields are shown in Fig.4 (a) and Fig.5 (a). Rydberg-EIT splits into several sub-peaks, the height of each sub-peak is different and entirely different splitting situations for two cases.

When we apply an axial magnetic field, the degenerate Zeeman sublevels will be shifted. For the Rydberg state $|3\rangle$, $|\mathrm{J},\ \mathrm{m}_J;\ \mathrm{I},\ \mathrm{m}_I\rangle$ basis is used as the eigenbasis while the $|\mathrm{F},\ \mathrm{m}_F\rangle$ as the eigenbasis for $|1\rangle$ and $|2\rangle$, as all the Zeeman sublevels of the cascade system shown in Fig.3 (b). The shifts of three levels $|1\rangle$, $|2\rangle$ and $|3\rangle$ are very different since the different magnetic interactions, just as our recent work [33]. The interval of adjacent Zeeman sublevels corresponding to $|1\rangle$, $|2\rangle$ and $|3\rangle$ levels can be expressed as:

$$\begin{aligned}\Delta_1 &= B\mu_B g_F(m_{F+1} - m_F) = 1/4\mu_B B \\ \Delta_2 &= B\mu_B g_F(m_{F+1} - m_F) = 2/5\mu_B B \\ \Delta_3 &= B\mu_B g_J(m_{J+1} - m_J) = 2\mu_B B\end{aligned} \tag{9}$$

Where μ_B=1.4MHz/G is the Bohr magneton, B is the magnetic field strength, g_J =3/2+[S(S+1)-L(L+1)]/[2J(J+1)] and g_F =g_J×[F(F+1)+J(J+1)-I(I+1)]/[2F(F+1)] are Lande g factor of $|\mathrm{J},\ \mathrm{m}_J;\ \mathrm{I},\ \mathrm{m}_I\rangle$ basis and $|\mathrm{F},\ \mathrm{m}_F\rangle$ basis, respectively.

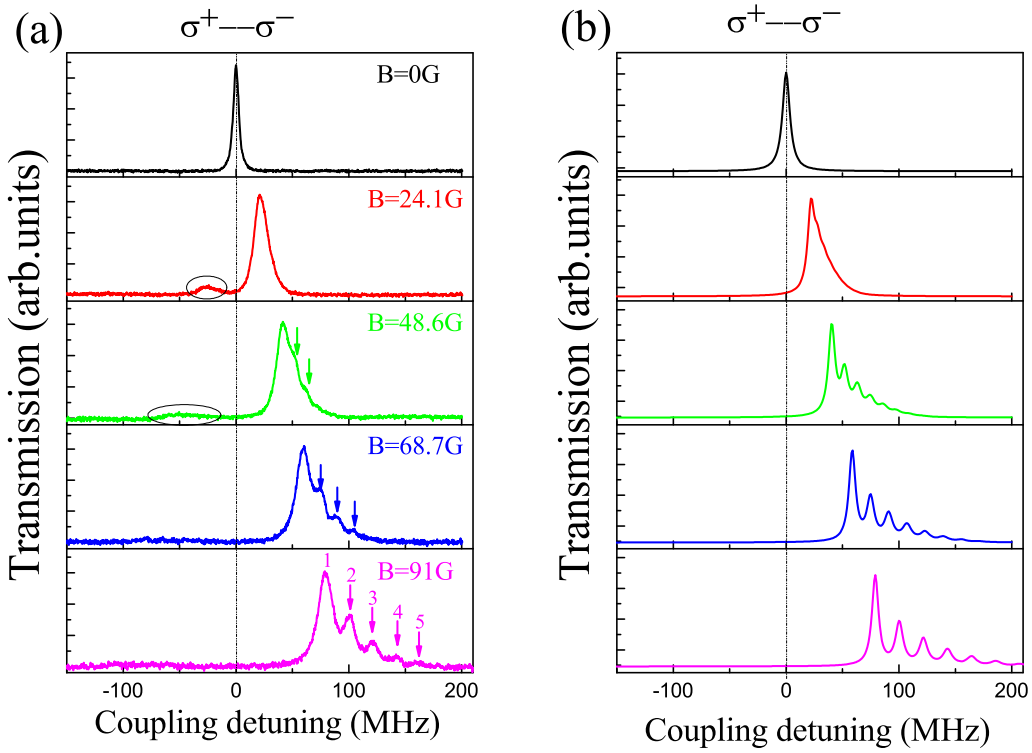

FIG. 4: (Color online) Measurements (a) and calculations (b) of Rydberg-EIT spectra with σ^+–σ^- polarization combination in different strength of magnetic field B, from 0 to 91G. With the increasing of magnetic field,splitting of Rydberg-EIT expand gradually. The number of distinguished sub-peaks and the interval between these sub-peaks increase gradually. We can only observe five sub-peaks at most, just as pink numbers, 1 to 5, when B=91G, which correspond to transitions {1} to {5}in Fig.3(b). Due to the limit of laser linewidth, the power and collision broadening in our experiments, the other sub-peaks corresponding to transitions {6} to {9} can't be observed.

All possible transitions coupled by circular polarized fields in the presence of an axial magnetic field are shown in Fig.3 (b). Nine possible cascade subsystems are formed for each circular polarization combination, σ^+–σ^- and σ^-–σ^+.In order to describe clearly, we number each subsystem as shown in Fig.3(b). For σ^+–σ^- case, number {1} to {8} correspond to the transitions $6S_{1/2}$(F=4, m_F)→$6P_{3/2}$(F'=5, m_F+1) →$49S_{1/2}$(F=4, m_J=1/2, m_I=7/2 to -7/2) (m_F=4 to -3), and number {9} corresponds to the transition $6S_{1/2}$(F=4, m_F)→$6P_{3/2}$(F'=5, m_F+1) →$49S_{1/2}$(F=4, m_J=-1/2, m_I=-7/2) (m_F=-4), while for σ^-–σ^+ case, number{$1^{'}$} corresponds to the transition $6S_{1/2}$(F=4, m_F)→$6P_{3/2}$(F'=5, m_F-1) →$49S_{1/2}$(F=4, m_J=-1/2, m_I=-7/2) (m_F=-4), and number{$2^{'}$} to {$9^{'}$} correspond to the transitions $6S_{1/2}$(F=4, m_F)→$6P_{3/2}$(F'=5, m_F-1) →$49S_{1/2}$(F=4, m_J=1/2, m_I=-7/2 to 7/2) (m_F=-3 to 4). Considering a subsystem, which corresponds to number{1}in Fig.3(b), consisting of $6S_{1/2}$(F=4, m_F=4), $6P_{3/2}$(F'=5, m'_F=5), $49S_{1/2}$(F=4, m_J=1/2, m_I=7/2), we have Δ_p= -4Δ_1+5Δ_2 and Δ_c= -5Δ_2+1/2Δ_3. Taking account of the Doppler effect that only are partially compensated by the counter-propagating beams, then Δ_p+Δ_c =(λ_p/λ_c-1)(-4Δ_1+5Δ_2)-5(λ_p/λ_c-1)Δ_2+1/2Δ_3 and the transmission peak should exist at Δ_c=(λ_p/λ_c-1)(-4Δ_1+5Δ_2)-5(λ_p/λ_c-1)Δ_2+1/2Δ_3 = -4*(852/510-1)Δ_1+1/2Δ_3 when we lock the probe laser on the resonance transition of $6S_{1/2}$(F=4)→ $6P_{3/2}$(F'=5). With the same approach, shifted amounts for all the other subsystems could be obtained. Therefore, we rewrite the χ, as Eq.6, for our experiments when the magnetic field is applied, as

$$\chi = \sum_{k=1}^{k=9} \int \chi(v)dv = \sum_{k=1}^{k=9} \quad \Downarrow$$
$$\int \frac{i\mu_{21}^2/\varepsilon_0\hbar}{\gamma_{21} - i\Delta_p - i\frac{\omega_p}{c}v + \frac{\Omega_c^2/4}{\gamma_{31}-i(\Delta_p+\Delta_c)-i(\omega_p-\omega_c)v/c}} N(v)dv \tag{10}$$

where k (from 1 to 9) correspond to one of nine cascade subsystems for each polarization combination, and μ_{21}, Δ_p, Δ_c, ω_{12}, ω_{23} will change accordingly for each k.

The numerically calculated Rydberg-EIT spectra in two kinds of polarization combinations with different magnetic fields using the revised theoretical expression Eq.(10) are shown in Fig.4 (b) and Fig.5 (b). It demonstrates polarization spectra in Rydberg-EIT,

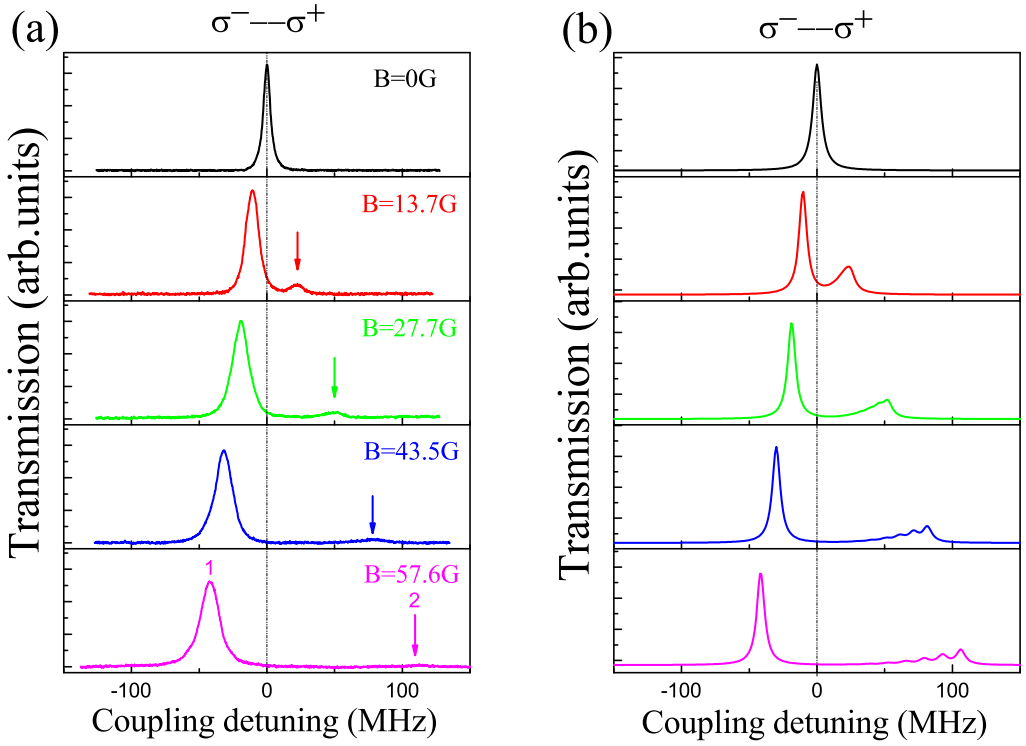

FIG. 5: (Color online) Measurements (a) and calculations (b) of Rydberg-EIT spectra with σ^-–σ^+ polarization combination in different strength of magnetic field B, from 0 to 57.6G. With the increasing of magnetic field,splitting of Rydberg-EIT expand gradually. We can only observe two sub-peaks at most, as pink numbers, 1 and 2, when B=57.6G. The left sub-peak at negative detuning, number 1, which corresponds to the transition $\{1'\}$in Fig.3(b). However, the right sub-peak at positive detuning is an envelope, which correspond to transitions $\{9'\}$ to $\{2'\}$in Fig.3(b). The main reasons for this envelope are the limit of laser linewidth, the power and collision broadening in our experiments.

and the simulation are well consistent with the experimental results. For σ^+–σ^- case, we can see the Rydberg-EIT spectra with different magnetic fields are very well consistent with experimental results except for the humps circled by black ellipse in 24.1G and 48.6G magnetic fields as shown in Fig.4(a). This is due to the imperfect polarization preparation in our experimens, which actually correspond to the transition $\{1'\}$ in Fig.3(b),$6S_{1/2}$(F=4, m_F=-4)→$6P_{3/2}$(F'=5, m'_F=-5) →$49S_{1/2}$(F=4, m_J=-1/2, m_I=-7/2), the left sub-peak at negative detuning in Fig.5. However, we can only observe an envelope for σ^-–σ^+ case in the experiments mainly because of the limit of laser linewidth, the power broadening and collision broadening in thermal vapors.

With the increasing of magnetic field, the number of distinguished sub-peaks and the interval between these sub-peaks increase gradually. The difference of polarization spectra for these two cases just result from the different strengths of dipole matrix elements between Zeeman sublevels for each subsystem. For σ^+–σ^- case, the strengths of dipole matrix elements are decreasing gradually from transition $\{1\}$ to $\{9\}$, so the profile of spectra is a slope, while for σ^-–σ^+ polarization combination, the strengths of dipole matrix elements of subsystems is "asymmetrical valley type" tendency. The transition $\{1'\}$, $6S_{1/2}$(F=4, m_F=-4) → $6P_{3/2}$(F'=5, m'_F=-5) → $49S_{1/2}$(F=4, m_J=-1/2, m_I =-7/2), the left sub-peak at negative detuning in Fig.5, has the largest dipole matrix element, while the second largest one, transition $\{2'\}$, $6S_{1/2}$(F=4, m_F=-3) → $6P_{3/2}$(F'=5, m'_F=-4) → $49S_{1/2}$(F=4, m_J=1/2, m_I=-7/2), is the rightmost sub-peak at positive detuning(still much less than the largest one), just like an asymmetrical valley.

Moreover, the frequency shift of each sub-peak varies proportionally with the strength of magnetic field, which is indicated by Eq. (9), as shown in Fig. 6, the polarization combination of probe and coupling fields is σ^+–σ^-. We also compare the frequency intervals between adjacent sub-peaks upon the fitting results with the theoretical values acquired by Eq. (9), as shown in Table.II, these sub-peaks are numbered as 1,2,3,4,5 as shown in Fig.4 (a), which correspond to the transitions $\{1\}$,$\{2\}$,$\{3\}$,$\{4\}$,$\{5\}$ in Fig.3(b),and then the intervals marked as δ_{12}, δ_{23}, δ_{34}, δ_{45}.δ_{ij} represents the frequency intervals between sub-peak i and sub-peak j, and there is a one-to-one correspondence between sub-peak i and transition{i}in Fig.3(b).The errors, maximum 4%, between theoretical prediction and the experiment data

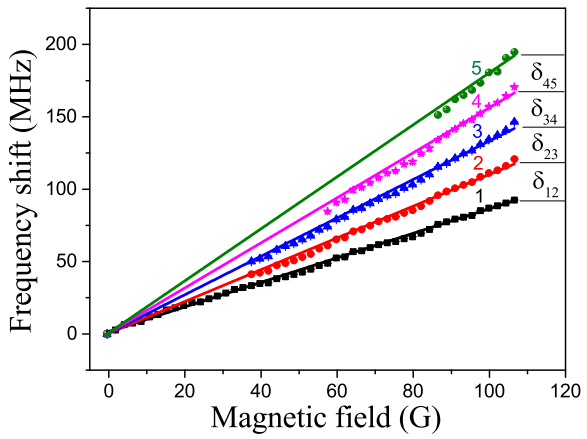

FIG. 6: (Color online) The frequency shifts of five sub-peaks in σ^+–σ^- polarization combination , black squares, red circles, blue triangles, pink stars and green spheres correspond to the sub-peak of 1,2,3,4,5 shown in Fig.4(a), which correspond to the transitions {1},{2},{3},{4},{5} in Fig.3(b), the solid lines are the linear fitting curves of experimental data. δ_{ij} represents the frequency intervals between sub-peak i and sub-peak j.

TABLE II: Experimental fitting and theoretical calculation of frequency intervals between adjacent sub-peak for σ^+–σ^- polarization combination. δ_{ij} represents the frequency intervals between sub-peak i and sub-peak j as shown in Fig.6

	Expt.	Cal.
δ_{12}	(0.2454±0.0032)B	0.2349B
δ_{23}	(0.2295±0.0040)B	
δ_{34}	(0.2292±0.0051)B	
δ_{45}	(0.2347±0.0052)B	

mainly result from the power broadening and collision broadening in thermal vapors.

V. CONCLUSION

We have observed the polarization spectra of Zeeman sublevels in Rydberg-EIT, involving degenerate Zeeman sublevels and nondegenerate Zeeman sublevels when an axial static magnetic field is applied. The essence of this magnitude dependence on probe and coupling field polarizations is that the presence of degenerate Zeeman sublevels and strength of relative dipole matrix elements between the Zeeman sublevels. However, the degeneracy will be broken and the splitting of Rydberg-EIT will present while an external magnetic field is applied. We investigate the polarization spectra of Rydberg-EIT in optimal polarization combinations when an external magnetic field is introduced. From a density matrix analysis of the cascade three-level system, we simulated the polarization spectra of Rydberg-EIT, and the theoretical simulation is shown to be good agreement with the experiment results. Finally,our work contributes to the more detailed understanding about the polarization of the optical fields and Zeeman Effect in Rydberg-EIT, which would be very attractive for optical bistability or applications in sensing, such as, vector microwave electrometry and a precision magnetometer .

VI. ACKNOWLEDGMENTS

The work was supported by State Key Development Program for Basic Research of China (Grant No.2012CB921603), NNSF of China (Grants Nos. 61378013, 91536110, 11274209, 61475090, 61505099), and NSF Grant No.PHY-1205559.

[1] M. O. Scully and M. S. Zubairy, *Quantum Optics* (Cambridge University Press, Cambridge, 1997), p. 225.
[2] A. Imamoglu and S. E. Harris, Opt. Lett. **14**, 1344 (1989).
[3] K. J. Boller, A. Imamoglu, and S. E. Harris, Phys. Rev. Lett. **66**, 2593 (1991).
[4] M. Xiao, Y. Q. Li, S. Z. Jin, and J. Gea-Banacloche, Phys. Rev. Lett. **74**, 666 (1995).
[5] S. A. Hopkins, E. Usadi, H. X. Chen, and A. V. Durrant, Opt. Commun. **138**, 185 (1997).
[6] L. V. Hau, S. E. Harris, Z. Dutton, and C. H. Behroozi, Nature **397**, 594 (1999).
[7] S. E. Harris and Lene Vestergaard Hau, Phys. Rev. Lett. **82**, 4611 (1999).
[8] K. Hakuta, L. Marmet, and B. P. Stoicheff, Phys. Rev. Lett. **66**, 596 (1991).
[9] M. M. Kash, V. A. Sautenkov, A. S. Zibrov, L. Hollberg, G. R. Welch, M. D. Lukin, Y. Rostovtsev, E. S. Fry, and M. O. Scully, Phys. Rev. Lett. **82**, 5229 (1999).
[10] M. D. Eisaman, A. André, F. Massou, M. Fleischhauer, A. S. Zibrov and M. D. Lukin, Nature **438**, 837 (2005).
[11] David Höckel and Oliver Benson, Phys. Rev. Lett. **105**, 153605 (2010).
[12] X. G. Wei, J. H. Wu, G. X. Sun, Z. Shao, Z. H. Kang, Y. Jiang, and J. Y. Gao, Phys. Rev. A. **72**, 023806 (2005).
[13] K. Cox, V. I. Yudin, A. V. Taichenachev, I. Novikova, and E. E. Mikhailov, Phys. Rev. A. **83**, 015801 (2011).
[14] T. F. Gallagher, *Rydberg Atoms* (Cambridge University Press, Cambridge, 1994), p. 1.
[15] M. L. Zimmerman, J. C. Castro, and D. Kleppner, Phys. Rev. Lett. **40**, 1083 (1978).
[16] M. L. Zimmerman, M. G. Littman, M. M. Kash, and D. Kleppner, Phys. Rev. A. **20**, 2251 (1979).
[17] J. A. Sedlacek, A. Schwettmann, H. Kübler, and J. P.

Shaffer, Phys. Rev. Lett. **111**, 063001 (2013).
[18] C. Carr, R. Ritter, C.G. Wade, C. S. Adams, and K. J. Weatherill, Phys. Rev. Lett. **111**, 113901 (2013).
[19] D. Jaksch, J. I. Cirac, P. Zoller ,S. L. Rolston, R. Côté and M. D. Lukin, Phys. Rev. Lett. **85**, 2208 (2000).
[20] E. Urban, T. A. Johnson, T. Henage, L. Isenhower, D. D. Yavuz, T. G. Walker and M. Saffman, Nature Phys. **5**, 110 (2009).
[21] A. Gaëtan, Y. Miroshnychenko, T. Wilk, A. Chotia, M. Viteau, D. Comparat, P. Pillet, A. Browaeys and P. Grangier, Nature Phys. **5**, 115 (2009).
[22] J. Clarke, H. Chen, and W. A. van Wijngaarden,Appl. Opt. **40**, 2047 (2001).
[23] A. K. Mohapatra, T. R. Jackson, and C. S. Adams, Phys. Rev. Lett. **98**, 113003 (2007).
[24] A. K. Mohapatra, M. G. Bason, B. Butscher, K. J. Weatherill, and C. S. Adams, Nature Phys. **4**, 890 (2008).
[25] M. Müller, I. Lesanovsky, H. Weimer, H. P. Büchler, and P. Zoller, Phys. Rev. Lett. **102**, 170502 (2009).
[26] H. Gorniaczyk, C. Tresp, J. Schmidt, H. Fedder, and S. Hofferberth, Phys. Rev. Lett. **113**, 053601 (2014).
[27] D. S. Ding, . C. S. Adams, B. S. Shi, and G. C. Guo, arXiv preprint arXiv:1606.08791 (2016).
[28] H. Zhang, L. Wang, J. Chen, S. Bao, L. Zhang, J. Zhao, and S. Jia, Phys. Rev. A. **87**, 033835 (2013).
[29] J. Gea-Banacloche, Y. Q. Li, S. Z. Jin, and M. Xiao, Phys. Rev. A. **51**, 576 (1995).
[30] D. Das and V. Natarajan, Europhys. Lett. **72**, 740 (2005).
[31] D. McGloin, M. H. Dunn, and D. J. Fulton, Phys. Rev. A. **62**, 053802 (2000).
[32] Daniel A. Steck, Cesium D Line Data (2010) p.9-10.
[33] S. Bao, W. Yang, H. Zhang, L. Zhang, J. Zhao, and S. Jia, J. Phys. Soc. Jpn **84**, 104301 (2015).